Solid State Ionics 309 (2017) 123–129

Contents lists available at ScienceDirect

Solid State Ionics

journal homepage: www.elsevier.com/locate/ssi

Ceria and $Ce_{0.95}M_{0.05}O_{2-\delta}$ mixed oxides (M = La, Pr, Zr): Vacancies and reducibility study

Ignacio Iglesias*, Graciela Baronetti, Fernando Mariño

Laboratorio de Procesos Catalíticos/Dpto. de Ingeniería Química/ITHES (UBA-CONICET)/Universidad de Buenos Aires, Ciudad Autónoma de Buenos Aires, Argentina

ARTICLE INFO

Keywords:
Doped ceria
Vacancies
Raman
OSC-OSCC

ABSTRACT

Highly reducible and redox active mixed oxides are employed in selective oxidation reactions and fuel cells, among others. Ceria is a renowned material in these applications because of its capacity to take and release oxygen. At the same time, these properties may be enhanced by cerium substitution with certain elements, usually, other rare earths. In this line, the present work is focused on the preparation of pure cerium oxide and doped with 5 %at of La, Pr or Zr. The solids were calcined at 600, 750 and 900 °C and characterized by diverse techniques (DRX, BET, Raman, OSC-OSCC, H_2-TPR).

When increasing calcination temperature, it was observed an improved specific surface and crystallite diameter conservation for La and Zr-doped samples. Oxygen vacancy generated by doping, observed both by Raman and OSC-OSCC, decreased with higher calcination temperatures for every solid. $Ce_{0.95}Pr_{0.05}O_{2-\delta}$ showed a maximum oxygen storage capacity for 750 °C calcination temperature consistent with Raman spectroscopy and hydrogen reduction profiles.

1. Introduction

Ceria based materials are extensively used in various catalytic applications where their ability to store/release oxygen is appreciated: three way catalysts where rapid response to feed conditions is required [1]; water gas shift supports where oxygen storage capacity (OSC) was correlated with catalytic activity [2]; carbon monoxide preferential oxidation where copper-ceria interaction provides high selectivity [3]; steam reforming where high oxygen mobility facilitates coke precursors gasification [4]; among others. Moreover, ceria distinctive properties may be enhanced by doping with small amounts of other elements, usually other rare earths.

Previous studies in our group, carried out by Poggio et al. [5], allowed identifying a maximum enhancement in ceria reducibility with 5%at Pr-doping. These results were later understood by means of theoretical calculations using a DFT approach [6], where a lower energy for vacancy generation was obtained for Pr-doped ceria. In accordance with Poggio et al., Ran et al. [7] also found maximum oxygen mobility in their Ce-Zr-Pr samples with 5%at Pr. Lanthanum doped ceria is an interesting system as well because intrinsic vacancies generated by cerium (Ce^{4+}) substitution with lanthanum cations (La^{3+}) may enhance oxygen mobility in the lattice [8] and, in addition, thermal stabilizing effect is expected for this solid solution [9]. On the other hand, zirconium doped ceria was extensively studied due to the possibility to synthesize solid solutions in all the composition range [10] and its unique properties regarding increased oxygen mobility, which were associated to bulk oxygen participation in redox processes [11]. Since zirconium ionic radii (0.84 Å) is smaller than cerium's (0.97 Å), the higher OSC measured for these solids was attributed to lattice distortion [12]. Benefits in doping are not always straightforward since increasing dopant concentration may cause defect interaction [13] or vacancy traps [14], which reduce oxygen mobility in the lattice. Taking this into consideration, an optimum dopant concentration is found in most systems. The solids prepared for this work are in the so-called dilute range, i.e. doping percentage is 5%at in every case, where defect interactions are expected to be negligible.

In order to develop better solids, deep understanding of their properties is required by means of different techniques. In this line, the present work deals with oxygen vacancies and samples' reducibility as characterized by Raman spectroscopy, OSC-OSCC and H_2-TPR, which are frequently used techniques in catalysis.

2. Experimental

2.1. Sample preparation

Previous results by our group showed that coprecipitation by homogeneous thermal decomposition of urea is a highly reproducible

* Corresponding author.
E-mail address: iiglesias@fi.uba.ar (I. Iglesias).

http://dx.doi.org/10.1016/j.ssi.2017.07.008
Received 2 May 2017; Received in revised form 7 June 2017; Accepted 10 July 2017

synthesis method for ceria based materials [15]. Therefore, samples in this work were prepared by this method, being the doping percentage (Zr, Pr, La) 5%at in every case. Aqueous solutions of urea, ceria and dopant nitrates were prepared with urea-cations ratio 10 to 1 and kept at 90 °C for 24 h. The precipitate obtained was washed and centrifuged three times before drying at 80 °C overnight. Afterwards, the solid was calcined at the desired temperature (600 °C, 750 °C or 900 °C) for 5 h in muffle.

2.2. Sample characterization

BET sortometry of samples calcined at 600 °C was performed using Micromeritics ASAP 2020 equipment, previously degassing for 24 h in Ar and using N_2 as adsorbate at − 196 °C. For solids calcined at higher temperatures (750 °C, 900 °C), taking in consideration the low specific surfaces expected, Kr was used as adsorbate in a Quantachrome Autosorb-1 equipment. XRD measurements were conducted in a Siemens D-501 diffractometer with Johansson Ge (111) monochromator, CuK alpha radiation, 45 kV and 35 mA. Raman spectra were collected using a LabRam (Horiba-Jobin-Yvon) spectrometer with an Olympus microscope equipped with × 100 objective and a CCD detector cooled at 200 K. Spectra Physics solid state laser of 532 nm and 30 mW was employed.

Micromeritics AutoChem II was used for H_2-TPR and OSC-OSCC measurements. Before starting any of these measurements, the solid surface was cleaned by flowing air at 450 °C for 30 min to eliminate any carbonates or adsorbed impurities usually present in these samples [16]. For H_2-TPR, mass employed was 50 mg, total gas flow 50 Nml/min (4% H_2/Ar) and temperature was raised from ambient to 1000 °C at 10 °C/min. For OSC and OSCC measurements at isothermal conditions (400 °C), the traditional method described by Yao and YuYao was followed [17]. In first place, alternate pulses of oxidant (air) and reductant (5% CO/Ar) were injected until stable CO_2 production was registered (OSC), i.e. typically 10 pulses. Afterwards, successive reductant pulses were injected until no CO_2 production was registered (OSCC).

3. Results and discussion

BET sortometry results are shown on Table 1 where it can be observed that specific surface areas for solids calcined at 600 °C were around 50 m^2/g while, for those calcined at 900 °C, specific surface area diminishes considerably, reaching values under 11 m^2/g. At the present preparation conditions, pure ceria had the largest surface area at 600 °C. When comparing samples calcined at 900 °C with those calcined at 600 °C, it can be observed La and Zr thermal stabilizing effect, as expected [9,18]. Solids calcined at 750 °C showed an intermediate BET surface value, closer to the one obtained for those calcined at 900 °C, i.e. BET surface diminution was higher in the first temperature increase, 600 °C to 750 °C. Similar values for pure and Pr-doped ceria were obtained at every calcination temperature in accordance with previous studies [19].

Table 1
BET area and XRD characterization results for samples calcined at different temperatures.

Sample	Calcination temperature (°C)	S_{BET} (m^2/g)	d_{XRD} (nm)	a_{XRD} (Å)	a_{Kim} (Å)	$a_{Hong\ y\ Virkar}$ (Å)
$CeO_{2-\delta}$	600	53.8	15	5.411	5.413	5.411
	750	8.01	104			
	900	6.03	138			
$Ce_{0.95}La_{0.05}O_{2-\delta}$	600	49.0	17	5.426	5.453	5.441
	750	12.0	70			
	900	8.57	98			
$Ce_{0.95}Pr_{0.05}O_{2-\delta}$	600	49.6	17	5.412	5.412	NA
	750	10.9	77			
	900	5.51	151			
$Ce_{0.95}Zr_{0.05}O_{2-\delta}$	600	44.1	19	5.410	5.399	NA
	750	14.8	60			
	900	10.6	79			

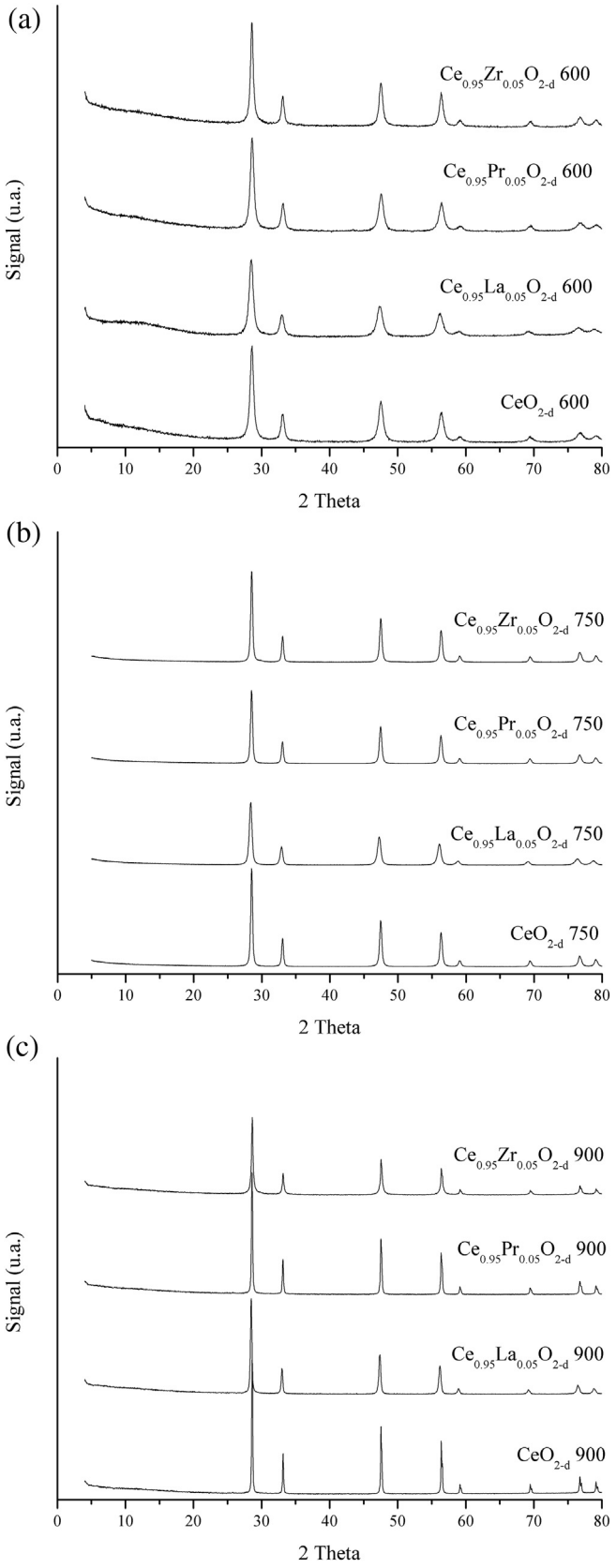

Fig. 1. XRD patterns of samples calcined at 600 °C (a), 750 °C (b) and 900 °C (c).

XRD patterns of the mixed oxides, exhibited in Fig. 1, showed typical reflections of ceria fluorite structure (JCPDS 34-0394). In addition, dopant oxides reflections were not observed which indicates, within XRD detection limits, the absence of any phase segregation for every sample, result which is consistent with the low doping percentage employed in this work (5%at). This result is in accordance with previous reports by other groups which successfully obtained solid solutions of Ce-La up to 50 %at [20], Ce-Pr up to 30%at [21] and Ce-Zr in all the composition range [22].

From XRD patterns, lattice parameters were obtained and they are shown in Table 1 next to theoretical values calculated with equations available in literature [23,24]. As it was expected, lattice parameters of ceria substituted with a higher radii cation (La^{+3}) were higher due to cell expansion while the opposite was true for lower radii cation dopant (Zr^{+4}). In the case of praseodymium doped ceria, since Pr^{+4} has almost the same radii than Ce^{+4}, lattice parameters were almost the same as well. It was observed that values obtained experimentally were in good agreement with theoretical estimations reinforcing solid solution formation (Hong and Vikar equation was only employed for trivalent dopants [24]).

Cerium oxide crystallite diameters (d_{XRD}) were estimated using Scherrer equation and are also shown in Table 1. At 600 °C, all samples had approximately the same d_{XRD} value, i.e. between 15 and 20 nm, and it increased considerably with increasing calcination temperature from 600 °C to 750 °C and 900 °C. This increase is not the same from every sample, being major for pure ceria and praseodymium doped ceria while both $Ce_{0.95}La_{0.05}O_{2-\delta}$ and $Ce_{0.95}Zr_{0.05}O_{2-\delta}$, the oxides which retained more specific surface area, showed the lowest d_{XRD}. These values were similar to the ones reported by other groups: Aneggi et al. [25] obtained 13 nm, 25 nm and 51 nm for ceria calcined at 600 °C, 700 °C and 800 °C, respectively; Zhou et al. [26] 12 nm, 43 nm and 114 nm at 600 °C, 750 °C and 900 °C; lower values were measured for La doped ceria [27], Pr doped ceria [28] and Zr doped ceria [29].

Raman spectra, presented in Fig. 2 for samples calcined at 600 °C, showed typical bands for ceria ascribed to F_{2g} mode at 465 cm^{-1}, main peak, and a secondary mixture of A_{1g}, E_g and F_{2g} modes (250 cm^{-1}, 570 $cm^{-1}$and 1170 cm^{-1} peaks) [30–32]. Additional secondary bands were observed by Pushkarev et al. [31] at 207 cm^{-1} and 428 cm^{-1} and by Spanier et al. [30] at 368 cm^{-1}, 600 cm^{-1} and 684 cm^{-1}. However, these bands were not distinguishable in our measurements. Zr-doped samples showed the same bands present in pure ceria as previously reported in literature [33–35], in spite of a minor band shift that will be commented afterwards. In the case of lanthanum and praseodymium doped ceria, same bands previously mentioned for ceria were observed as expected from earlier reports [36–43] and an additional peak was detected at 190 cm^{-1}, which Luo et al. attributed to asymmetrical oxygen vacancies vibration since its behavior was analogous to 570 cm^{-1} band [38]. In the case of praseodymium doped ceria, another peak at 960 cm^{-1} was observed which might be associated to Pr_6O_{11} phase [44], which was not detected by XRD probably due to its low content.

Table 2 shows main band position, F_{2g} vibration mode, and I_{570}/I_{465} intensity ratio for every sample. The band observed at 570 cm^{-1} is usually associated to oxygen vacancies [45] and, consequently, the intensity ratio between this band and the main band (I_{570}/I_{465}) was calculated to follow vacancies evolution with calcination temperature and doping. As it may be observed, for both calcination temperatures, main band position shifts to lower values in doped samples what may be attributed to two effects: lattice parameter contraction and/or vacancies creation in these materials. Band shift ascribed to lattice parameter modification may be theoretically calculated by the following equation:

$$\Delta\omega_a = -3\gamma\omega_0\Delta a/a_0$$

where $CeO_{2-\delta}$ 600 was considered as reference for ω_0 (reference band position) and a_0 (reference lattice parameter) and γ is Grünesian constant, taken equal to 1.24 [46].On the other hand, oxygen vacancies induce a negative band shift. Thus, in the case of lanthanum doped samples, for which lattice expands (see Table 1), negative band shift is attributed to predominance of the vacancies effect. Following McBride et al. [46], if lattice parameter induced band shift ($\Delta\omega_a$) is subtracted from the one observed, remaining shift may be associated to oxygen vacancies formation in the solid ($\Delta\omega_{V_o}$). These values are shown in Table 2 as well.

Regarding I_{570}/I_{465} intensity ratio, it may be observed that there was a minor decrease in oxygen vacancies when calcination temperature was increased, which is in line with OSC and OSCC results discussed below. Vacancies diminution with increasing calcination temperature was in agreement with previous results from our group by Poggio et al. [16]. In their work, the authors used XPS to determine superficial oxidation state of $CeO_{2-\delta}$ calcined at different temperatures and found an almost linear decrease of Ce^{3+} with calcination temperature, i.e. increasing oxidation state or lower vacancy concentration. The higher I_{570}/I_{465} values calculated for Pr-doped samples are related to absorbance phenomenon with laser employed and should not be interpreted as an unusually high vacancy concentration in these samples. Since laser absorbance is higher for the colored Pr containing solids, information obtained was more representative of the solid surface where vacancies are concentrated as previously observed by Poggio et al. [5] and Luo et al. [46]. Noteworthy, a maximum in I_{570}/I_{465} was observed for $Ce_{0.95}Pr_{0.05}O_{2-\delta}$ 750 which was in accordance with OSC-OSCC results and H_2-TPR measurements as will be shown below. This might be related to the appearance of the band at 960 cm^{-1}, ascribed tentatively to Pr_6O_{11} that, in fact, also shows a maximum intensity at intermediate calcination temperature as shown in Table 2 and Figure 3.

Regarding vacancies associated shift ($\Delta\omega_{V_o}$), firstly it should be emphasized the fact that positive values indicate less vacancies than reference while the opposite is true for negative ones. Therefore, it was observed this value increased for every sample with calcination temperature in accordance with the increasing I_{570}/I_{465} ratio. In addition, it was seen that the higher vacancies shifts were calculated for lanthanum doped ceria for which intrinsic vacancies generation was expected as a consequence of cerium substitution. Comparing doped samples with pure ceria at the same calcination temperature, higher vacancy concentration was observed for almost every sample which, taking into account solids synthesized are in the dilute range, it is desirable in view of oxygen mobility enhancement.Table 3 shows the results obtained for OSC and OSCC measurements for the samples prepared. At the same time, following Rossignol et al. [39], a theoretical calculation of OSC taking in consideration geometrical aspects is provided:

$$OSC_{Calc.} = \frac{S_{BET}\ b}{N_{Av}\ a_{XRD}{}^2}$$

where S_{BET} is the surface area, b the reducible cations fraction (1 for $CeO_{2-\delta}$ and $Ce_{0.95}Pr_{0.05}O_{2-\delta}$; 0.95 for $Ce_{0.95}La_{0.05}O_{2-\delta}$ and $Ce_{0.95}Zr_{0.05}O_{2-\delta}$), N_{Av} the Avogadro's number and a_{XRD} the lattice parameter. From the previous equation, the superficial character of OSC for which S_{BET} value limits available oxygen may be noticed while, on the contrary, since OSCC is measured to full reduction of the solid, bulk oxygen is expected to participate. Values reported in Table 3 were in accordance with previous results obtained by other groups [14,47,48]. For instance, when studying pure ceria, Madier et al. [47] measured 76 μmol CO_2/g (OSC) and 112 μmol CO_2/g (OSCC) while Aneggi et al. [48] found 40 μmol CO_2/g (OSC). Table 3 shows that measured OSCC values decreased for every formulation with calcination temperature, except for $Ce_{0.95}Pr_{0.05}O_{2-\delta}$, in line with vacancies analysis by Raman spectroscopy presented above. In spite of oxygen vacancies present in $Ce_{0.95}La_{0.05}O_{2-\delta}$, since BET surface area diminution was observed for the solid calcined at 600 °C (Table 1), OSC values resulted the same for La doped and pure ceria at that calcination temperature. Considering that samples containing Zr have no intrinsic vacancies, oxygen mobility

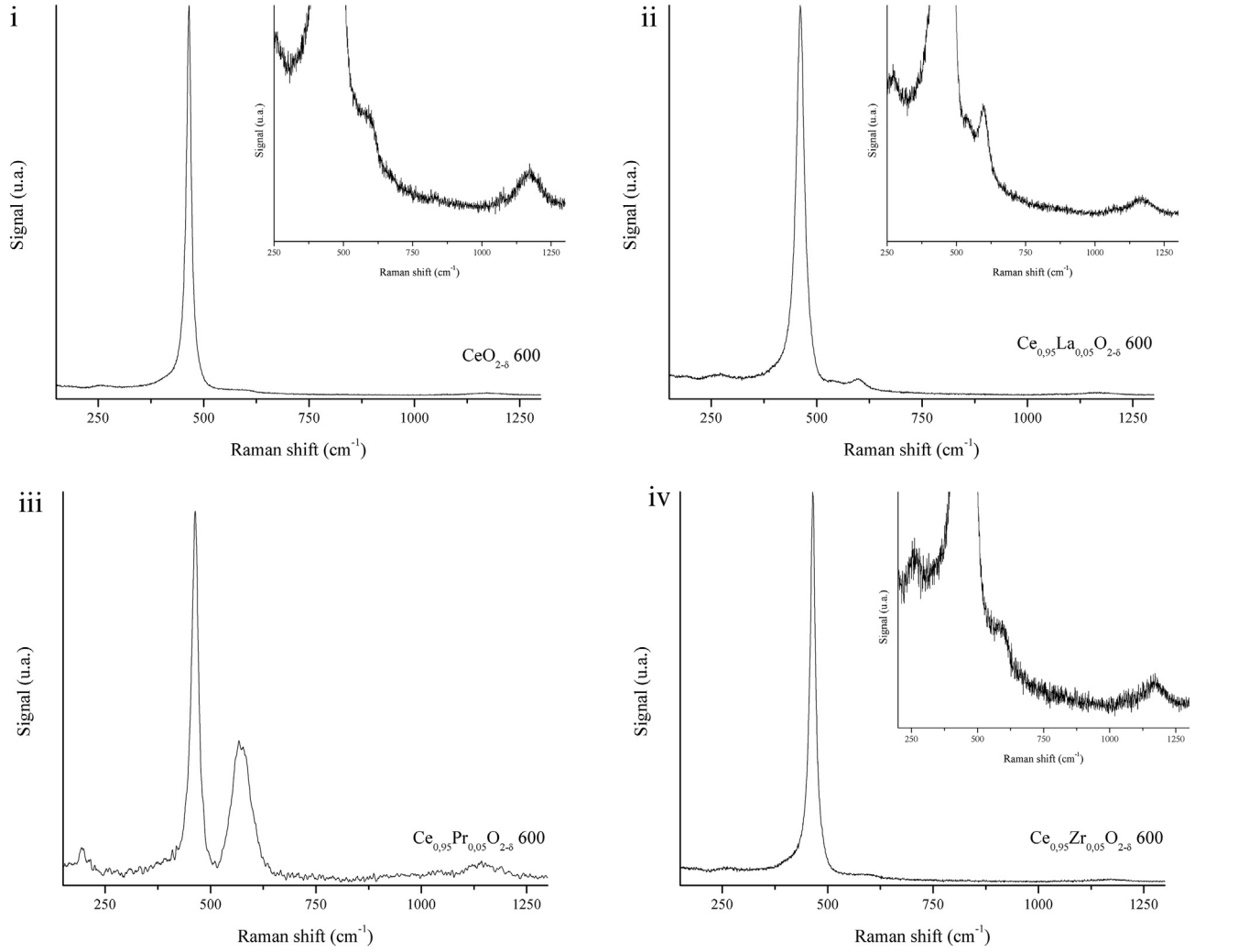

Fig. 2. Raman spectra for samples calcined at 600 °C.

Table 2
Raman characterization results for samples calcined at different temperatures.

Sample	Calcination temperature (°C)	F_{2g} main band position (cm^{-1})	$I_{570}/I_{F_{2g}}$ (%)	$I_{960}/I_{F_{2g}}$ (%)	$\Delta\omega_{V_{\ddot{O}}}$ (cm^{-1})
$CeO_{2-\delta}$	600	465	1.3		0
	750	466	0.7		1
	900	467	0.0		2
$Ce_{0.95}La_{0.05}O_{2-\delta}$	600	461	3.8		−9
	750	462	3.2		−8
	900	463	3.0		−7
$Ce_{0.95}Pr_{0.05}O_{2-\delta}$	600	464	37.1	1.6	−2
	750	464	38.6	3.4	−1
	900	465	35.1	3.1	1
$Ce_{0.95}Zr_{0.05}O_{2-\delta}$	600	464	1.8		−1
	750	467	0.9		2
	900	467	1.0		2

enhancement is justified by means of differences in cation size between Zr^{+4} and cerium which may generate lattice distortion. Moreover, oxygen diffusion should be easier in a smaller cell [49]. It may be observed from Table 3 that Zr-doped samples' OSC almost doubled pure ceria at every calcination temperature. Nevertheless, OSC values always remained below calculated ones and, therefore, bulk oxygen contribution to OSC could not be assured. In the case of praseodymium, previous results of our group had already exhibit an increase in oxygen

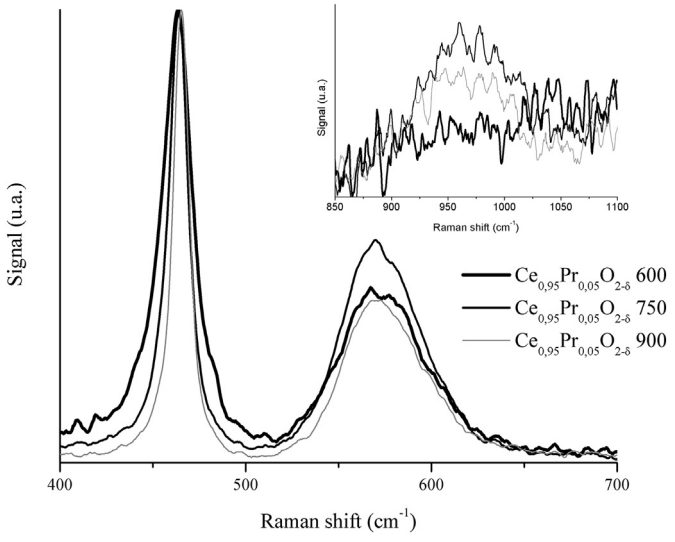

Fig. 3. Raman spectra for $Ce_{0.95}Pr_{0.05}O_{2-\delta}$ at calcined at different temperatures.

mobility when doping ceria even with small quantities of Pr in materials calcined at 450 °C [5,6]. In the present work, for samples calcined at 750 °C and 900 °C, the greatest OSC and OSCC values were registered for $Ce_{0.95}Pr_{0.05}O_{2-\delta}$ while at 600 °C, Pr-doped sample was only

Table 3
OSC-OSCC results for samples calcined at different temperatures.

Sample	Calcination temperature (°C)	OSC (μmol CO_2/g)	OSCC (μmol CO_2/g)	$OSC_{Calc.}$ (μmol CO_2/g)
$CeO_{2-\delta}$	600	48	123	305
	750	27	85	45
	900	19	34	34
$Ce_{0.95}La_{0.05}O_{2-\delta}$	600	48	122	263
	750	30	65	64
	900	19	36	46
$Ce_{0.95}Pr_{0.05}O_{2-\delta}$	600	63	147	281
	750	76	165	62
	900	56	149	31
$Ce_{0.95}Zr_{0.05}O_{2-\delta}$	600	82	202	238
	750	55	123	80
	900	38	80	57

overcome by $Ce_{0.95}Zr_{0.05}O_{2-\delta}$. It is worth mentioning that $Ce_{0.95}Pr_{0.05}O_{2-\delta}$ 750 had a bigger OSC than $Ce_{0.95}Pr_{0.05}O_{2-\delta}$ 600 even with a lower surface area (Table 1), in accordance with Raman results (Table 2). In addition, OSC measured for $Ce_{0.95}Pr_{0.05}O_{2-\delta}$ 900 is remarkable when comparing it with $Ce_{0.95}Pr_{0.05}O_{2-\delta}$ 600, considering surface area of the latter is 9 times higher. As it will be discussed below, these results are also in agreement with H_2-TPR results where $Ce_{0.95}Pr_{0.05}O_{2-\delta}$ was the only solid to retain low temperature reduction activity at high calcination temperature.

H_2-TPR profiles for the samples calcined at different temperatures are shown in Fig. 4 while deconvolution results are presented in Table 4. Two reduction zones were observed, in agreement with previous publications on doped [5,50,51] and pure ceria [52,53]: low temperature region corresponds to surface reduction (α Peak) while high temperature region is usually identified with bulk reduction (δ Peak). There was an additional event (β Peak) at the low temperature region for $Ce_{0.95}Pr_{0.05}O_{2-\delta}$ that retained certain hydrogen consumption even for the 900 °C-calcined sample. This event may be related to a different kind of oxygen species in this sample in which both cations (host: Ce and dopant: Pr) have two possible oxidation states [6] or it could be ascribed to the presence of Pr_6O_{11} for which other authors reported similar temperatures of reduction: Luo et al. (530 °C) [46], Logan and Shelef (550 °C) [54] and Long et al. (560 °C) [55].

Concerning α Peak, it was observed a linear relationship between hydrogen consumed and BET area for every sample, regardless the dopant in the mixed oxide, reinforcing the superficial character of this reduction event and in line with previous results by other authors [56]. In fact, low temperature reduction almost disappeared for samples calcined at 900 °C. With regard to total hydrogen consumption, it was observed that this amount descended with the increase in calcination temperature for every sample as expected. Reducibility for La-doped and Zr-doped supports was lower than that of pure ceria, which may be explained by the diminution of reducible material when doping with non reductible cations such as La^{+3} and Zr^{+4}. On the other hand, Pr has two different oxidation states and it is known to enhance ceria reduction [5,6], thus its reducibility may be higher as it was the case for samples calcined at 600 °C. It may also be noted from Fig. 4 that bulk reduction (δ Peak) started at lower temperatures for doped ceria at every calcination temperature, indicating bulk oxygen mobility promotion due to dopant effect as previously observed with OSCC results (Table 3). When considering α Peak temperature in every sample, it may be observed that superficial reduction became increasing difficult for higher calcination temperatures in line with OSC results. In addition, regarding $Ce_{0.95}Pr_{0.05}O_{2-\delta}$, a minimum in α Peak temperature with calcination temperature is evident, in agreement with enhanced reducibility observed in OSC experiments as well.

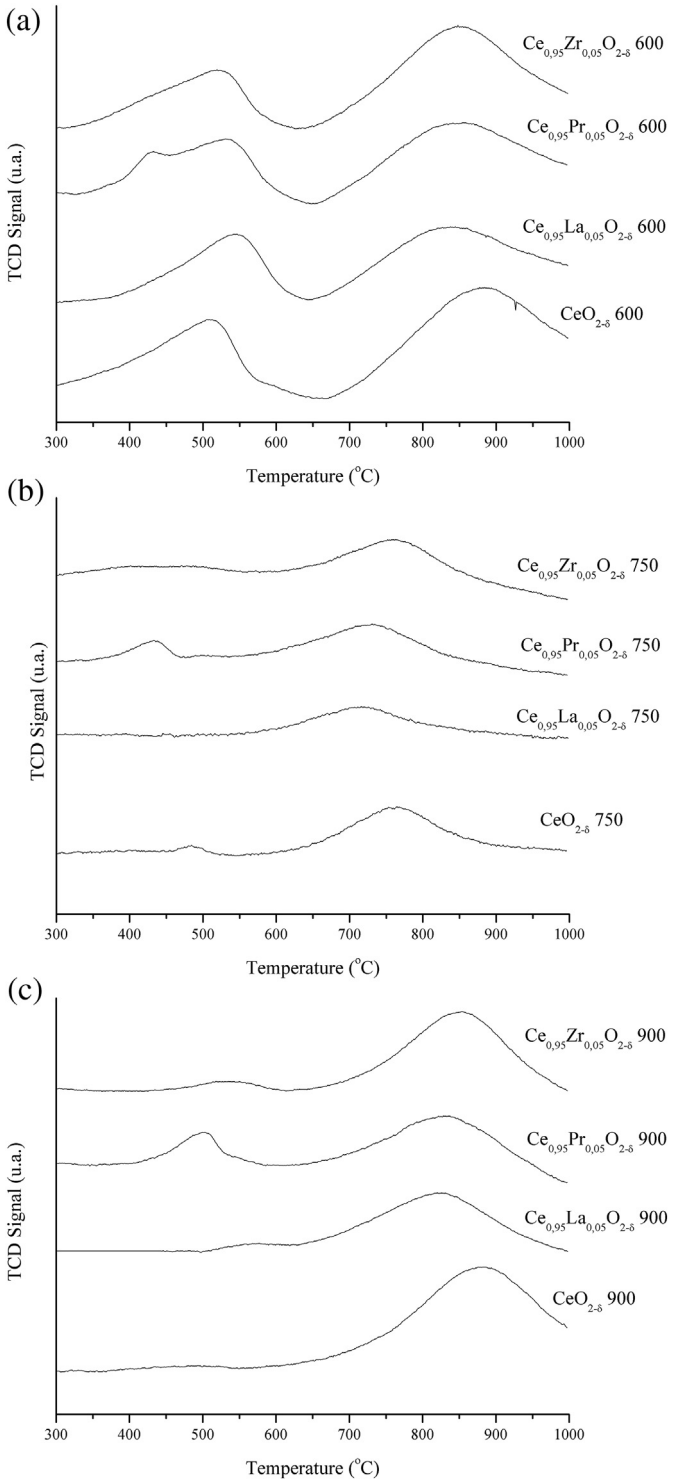

Fig. 4. H_2-TPR profiles for samples calcined at 600 °C (a), 750 °C (b) and 900 °C (c).

4. Conclusions

Samples prepared at different calcination temperatures (600 °C, 750 °C and 900 °C) were characterized by means of BET, XRD, Raman, OSC-OSCC and H_2-TPR. They all showed ceria fluorite structure with no dopant phase segregation and lattice parameter calculated was in accordance with solid solution formation in every case. Zr and La-doped supports were the ones to retain more BET area (lower crystallite diameter) when increasing calcination temperature while Pr-doped samples showed similar values to pure ceria. All doped samples showed

Table 4
H_2-TPR deconvolution results for samples calcined at different temperatures.

Sample	Calcination temperature (°C)	α peak		β peak	δ peak	H_2 total consumption (μmol/g)
		T (°C)	H_2 consumption (μmol/g)	T (°C)	T (°C)	
$CeO_{2-\delta}$	600	480	409	–	886	1273
	750	484	13	–	785	1063
	900	488	6	–	878	863
$Ce_{0.95}La_{0.05}O_{2-\delta}$	600	524	281	–	849	789
	750	605	89	–	716	530
	900	608	74	–	819	517
$Ce_{0.95}Pr_{0.05}O_{2-\delta}$	600	452	436	543	860	1543
	750	426	105	531	727	911
	900	493	80	555	827	634
$Ce_{0.95}Zr_{0.05}O_{2-\delta}$	600	492	321	–	854	1141
	750	511	44	–	762	770
	900	533	30	–	845	536

increased reducibility in comparison to pure ceria, particularly Zr and Pr-doped ones. Oxygen vacancies and reducibility were assessed by different techniques and proven to decrease with higher calcination temperatures. The case of $Ce_{0.95}Pr_{0.05}O_{2-\delta}$ deserved further attention since a maximum in 570 cm^{-1} Raman band intensity and OSC with calcination temperature was measured. Furthermore, it was the only sample to preserve reduction activity at low temperature when calcined at 900 °C. This observation, in addition to the appearance of 960 cm^{-1} Raman band, may indicate the formation of Pr_6O_{11} which would be responsible for the exceptional reducibility in this sample.

Acknowledgments

Ignacio Iglesias is thankful to J. R. Garcia and U. Sedrán for low BET area measurements at INCAPE, J. Múnera for his assistance in Raman spectroscopy measurements and FIUBA for his Peruilh doctoral grant.

References

[1] A. Trovarelli, Catalysis by Ceria and Related Materials, Imperial College Press, London, 2002.
[2] L. Cao, C. Ni, Z. Yuan, S. Wang, Correlation between catalytic selectivity and oxygen storage capacity in autothermal reforming of methane over Rh/$Ce_{0.45}Zr_{0.45}RE_{0.1}$ catalysts (RE = La, Pr, Nd, Sm, Eu, Gd, Tb), Catal. Commun. 10 (2009) 1192–1195.
[3] F. Mariño, B. Schönbrod, M. Moreno, M. Jobbágy, G. Baronetti, M. Laborde, CO preferential oxidation over CuO–CeO_2 catalysts synthesized by the urea thermal decomposition method, Catal. Today 133–135 (2008) 735–742.
[4] S.D. Angeli, G. Monteleone, A. Giaconia, A.A. Lemonidou, State-of-the-art catalysts for CH_4 steam reforming at low temperature, Int. J. Hydrog. Energy 39 (2014) 1979–1997.
[5] E. Poggio, F. Mariño, M. Laborde, G. Baronetti, Copper and nickel catalysts supported on praseodymium-doped ceria (PDC) for the water-gas shift reaction, Appl. Catal. A Gen. 460–461 (2013) 15–20.
[6] E. Poggio, B. Irigoyen, G. Baronetti, F. Mariño, Ce-Pr mixed oxides as active supports for water-gas shift reaction: experimental and density functional theory characterization, Appl. Catal. A Gen. 485 (2014) 123–132.
[7] R. Ran, D. Weng, X. Wu, J. Fan, L. Wang, X. Wu, Structure and oxygen storage capacity of Pr-doped $Ce_{0.26}Zr_{0.74}O_2$ mixed oxides, J. Rare Earths 29 (2011) 1053–1059.
[8] S. Dikmen, P. Shuk, M. Greenblatt, Hydrothermal synthesis and properties of $Ce_{1-x}La_xO_{2-\delta}$ solid solutions, Solid State Ionics 126 (1999) 89–95.
[9] C.M. Kalamaras, K.C. Petallidou, A.M. Efstathiou, The effect of La^{3+}-doping of CeO_2 support on the water-gas shift reaction mechanism and kinetics over Pt/$Ce_{1-x}La_xO_{2-\delta}$, App. Cat. B 136–137 (2013) 225–238.
[10] F. Zhang, C.-H. Chen, J.C. Hanson, R.D. Robinson, I.P. Herman, S.-W. Chan, Phases in ceria–zirconia binary oxide (1 − x)CeO_2–xZrO_2 nanoparticles: the effect of particle size, J. Am. Ceram. Soc. 89-3 (2006) 1028–1036.
[11] D. Duprez, Study of surface reaction mechanisms by $^{16}O/^{18}O$ and H/D isotopic exchange, Catal. Today 112 (2006) 17–22.
[12] S. Bedrane, C. Descorme, D. Duprez, Towards the comprehension of oxygen storage processes on model three-way catalysts, Catal. Today 73 (2002) 233–238.
[13] J. Faber, C. Geoffroy, A. Roux, A. Sylvestre, P. Abelard, A systematic investigation of the dc electrical conductivity of rare-earth doped ceria, Appl. Phys. A Mater. Sci. Process. 49 (1989) 225–232.
[14] P.P. Dholabhai, S. Anwar, J.B. Adams, P. Crozier, R. Sharma, Kinetic lattice Monte Carlo model for oxygen vacancy diffusion in praseodymium doped ceria: applications to materials design, J. Solid State Chem. 184 (2011) 811–817.
[15] M. Jobbágy, F. Mariño, B. Schönbrod, G. Baronetti, M.A. Laborde, Synthesis of copper-promoted CeO_2 catalysts, Chem. Mater. 18 (2006) 1945–1950.
[16] E. Poggio, M. Jobbágy, M. Moreno, M. Laborde, F. Mariño, G. Baronetti, Influence of the calcination temperature on the structure and reducibility of nanoceria obtained from crystalline $Ce(OH)CO_3$ precursor, IJHE 18 (2011) 15899–15905.
[17] H.C. Yao, Y.F. Yu Yao, Ceria in automotive exhaust catalysts: I. Oxygen storage, J. Catal. 86 (1984) 254–265.
[18] J. Chen, Q. Wua, J. Zhang, J. Zhang, Effect of preparation methods on structure and performance of Ni/$Ce_{0.75}Zr_{0.25}O_2$ catalysts for CH_4–CO_2 reforming, Fuel 87 (2008) 2901–2907.
[19] Z. Song, W. Liu, H. Nishiguchi, A. Takami, K. Nagaoka, Y. Takita, The Pr promotion effect on oxygen storage capacity of Ce–Pr oxides studied using a TAP reactor, Appl. Catal. A Gen. 329 (2007) 86–92.
[20] S. Liang, E. Broitman, Y. Wang, A. Cao, G. Veser, Highly stable, mesoporous mixed lanthanum–cerium oxides with tailored structure and reducibility, J. Mater. Sci. 46 (2011) 2928–2937.
[21] M.A. Vasiliades, M.M. Makri, P. Djinovic, B. Erjavec, A. Pintar, A.M. Efstathiou, Dry reforming of methane over 5 wt% Ni/$Ce_{1-x}Pr_xO_2$ catalysts: performance and characterisation of active and inactive carbon by transient isotopic techniques, Appl. Catal. B Environ. 197 (2016) 168–183.
[22] T. Tsoncheva, R. Ivanova, J. Henych, M. Dimitrov, M. Kormunda, D. Kovacheva, N. Scotti, V. Dal Santo, V. Stengl, Effect of preparation procedure on the formation of nanostructured ceria–zirconia mixed oxide catalysts for ethyl acetate oxidation: homogeneous precipitation with urea vs template-assisted hydrothermal synthesis, Appl. Catal. A Gen. 502 (2015) 418–432.
[23] D. Kim, Lattice parameters, ionic conductivities, and solubility limits in fluorite-structure MO_2 Oxide (M = Hf^{4+}, Zr^{4+}, Ce^{4+}, Th^{4+},U^{4+}) solid solutions, J. Am. Ceram. Soc. 72 (1989) 1415–1421.
[24] S.J. Hong, A.V. Virkar, Lattice parameters and densities of rare-earth oxide doped ceria electrolytes, J. Am. Ceram. Soc. 78 (1995) 433–439.
[25] E. Aneggi, J. Llorca, M. Boaro, A. Trovarelli, Surface-structure sensitivity of CO oxidation over polycrystalline ceria powders, J. Catal. 234 (2005) 88–95.
[26] X.-D. Zhou, W. Huebner, H.U. Anderson, Room-temperature homogeneous nucleation synthesis and thermal stability of nanometer single crystal CeO_2, Appl. Phys. Lett. 80-20 (2002) 3814–3816.
[27] X. Hou, Y. Xue, N. Han, Q. Lu, X. Wang, M.-H. Phan, Y. Zhong, Nanocrystalline $Ce_{1-x}La_xO_{2-d}$ solid solutions synthesized by hydrolyzing and oxidizing, J. Electron. Mater. 45-5 (2016) 2559–2562.
[28] J. Yang, Z.-F. Zhu, J.-P. Li, Influence of Preparation Temperature on Performance of $Ce_{1-x}Pr_xO_2$ Ultrafine Powder Prepared by a Microemulsion Process, Key Eng. Mater. 368 (2008) 784–786.
[29] E. Mamontov, T. Egami, R. Brezny, M. Koranne, S. Tyagi, Lattice defects and oxygen storage capacity of nanocrystalline ceria and ceria-zirconia, J. Phys. Chem. B 104 (2000) 11110–11116.
[30] J.E. Spanier, R.D. Robinson, F. Zhang, S.-W. Chan, I.P. Herman, Size-dependent properties of CeO_{2-y} nanoparticles as studied by Raman scattering, Phys. Rev. B 64 (2001) (245407-7).
[31] V.V. Pushkarev, V.I. Kovalchuk, J.L. d'Itri, Probing defect sites on the CeO_2 surface with dioxygen, J. Phys. Chem. B 108 (2004) 5341–5348.
[32] W.H. Weber, K.C. Bass, J.R. McBride, Raman study of CeO_2. Second-order scattering, lattice dynamics, and particle-size effects, Phys. Rev. B 48-1 (1993) 178–185.
[33] M. Kuhn, S.R. Bishop, J.L.M. Rupp, H.L. Tullera, Structural characterization and oxygen nonstoichiometry ofceria-zirconia ($Ce_{1-x}Zr_xO_{2-\delta}$) solid solutions, Acta Mater. 61 (2013) 4277–4288.
[34] A.M. Bolon, M.M. Gentleman, Raman spectroscopic observations of ferroelastic switching in ceria-stabilized zirconia, J. Am. Ceram. Soc. 94-12 (2011) 4478–4482.
[35] T. Merle, R. Guinebretiere, A. Mirgorodsky, P. Quintard, Polarized Raman spectra of tetragonal pure ZrO_2 measured on epitaxial films, Phys. Rev. B65 (2002) 144302–144306.

[36] G.-Q. Xie, M.-F. Luo, M. He, P. Fang, J.-M. Ma, Y.-F. Ying, Z.-L. Yan, An improved method for preparation of $Ce_{0.8}Pr_{0.2}O_Y$ solid solutions with nanoparticles smaller than 10 nm, J. Nanopart. Res. 9 (2007) 471–478.
[37] Z.-Y. Pu, J.-Q. Lu, M.-F. Luo, Y.-L. Xie, Study of oxygen vacancies in $Ce_{0.9}Pr_{0.1}O_{2-\delta}$ solid solution by in situ X-ray diffraction and in situ Raman spectroscopy, J. Phys. Chem. C 111 (2007) 18695–18702.
[38] M.-F. Luo, Z.-L. Yan, L.-Y. Jin, Structure and redox properties of $Ce_xPr_{1-x}O_{2-\delta}$mixed oxides and their catalytic activities for CO, CH_3OH and CH_4 combustion, J. Mol. Catal. A Chem. 260 (2006) 157–162.
[39] S. Rossignol, F. Gérard, D. Mesnard, C. Kappenstein, D. Duprez, Structural changes of Ce–Pr–O oxides in hydrogen: a study by in situ X-ray diffraction and Raman spectroscopy, J. Mater. Chem. 13 (2003) 3017–3020.
[40] L. Katta, P. Sudarsanam, G. Thrimurthulu, B.M. Reddy, Doped nanosized ceria solid solutions for low temperature soot oxidation: zirconium versus lanthanum promoters, Appl. Catal. B Environ. 101 (2010) 101–108.
[41] H. Li, G. Lu, Y. Wang, Y. Guo, Synthesis of flower-like La or Pr-doped mesoporous ceria microspheres and their catalytic activities for methane combustion, Catal. Commun. 11 (2010) 946–950.
[42] C.E. Jeyanthi, R. Siddheswaran, P. Kumar, V.S. Shankar, K. Rajarajan, Structural and spectroscopic studies of rare earths doped ceria ($RE_{La,Sc,Yb}$:CeO_2) nanopowders, Ceram. Int. 40 (2014) 8599–8605.
[43] D.W. Wheeler, I. Khan, A Raman spectroscopy study of cerium oxide in a cerium–5 wt.% lanthanum alloy, Vib. Spectrosc. 70 (2014) 200–206.
[44] J. Hyodo, K. Tominaga, S. Idaab, T. Ishihara, Effects of three-dimensional mechanochemical tensile strain on fast oxygen diffusion in Audispersed $Pr_{1.90}Ni_{0.71}Cu_{0.24}Ga_{0.05}O_4$, J. Mater. Chem. A 4 (2016) 3844–3849.
[45] J.R. McBride, K.C. Hass, B.D. Poindexter, W.H. Weber, Raman and X-ray studies of $Ce_{1-x}RE_xO_{2-y}$, where RE = La, Pr, Nd, Eu, Gd, and Tb, J. Appl. Physics 76 (1994) 2435–2441.
[46] M.-F. Luo, Z.-L. Yan, L.-Y. Jin, M. He, Raman spectroscopic study on the structure in the surface and the bulk Shell of $Ce_xPr_{1-x}O_{2-\delta}$ mixed oxides, J. Phys. Chem. B 110 (2006) 13068–13071.
[47] Y. Madier, C. Descorme, A.M. Le Govic, D. Duprez, Oxygen mobility in CeO_2 and $Ce_xZr_{(1-x)}O_2$ compounds: study by CO transient oxidation and $^{18}O/^{16}O$ isotopic exchange, J. Phys. Chem. B 103 (1999) 10999–11006.
[48] E. Aneggi, M. Boaro, C. de Leitenburg, G. Dolcetti, A. Trovarelli, Insights into the dynamics of oxygen storage/release phenomena in model ceria–zirconia catalysts as inferred from transient studies using H_2, CO and soot as reductants, Catal. Today 112 (2006) 94–98.
[49] G.R. Rao, B.J. Mishra, Structural, redox and catalytic chemistry of ceria based materials, Bull. Catal. Soc. India 2 (2003) 122–134.
[50] A. Kambolis, H. Matralis, A. Trovarelli, Ch. Papadopoulou, Ni/CeO_2-ZrO_2 catalysts for the dry reforming of methane, Appl. Catal. A Gen. 377 (2010) 16–26.
[51] B. Zhang, D. Li, X. Wang, Catalytic performance of La–Ce–O mixed oxide for combustion of methane, Catal. Today 158 (2010) 348–353.
[52] F. Giordano, A. Trovarelli, C. de Leitenburg, M. Giona, A model for the temperature-programmed reduction of low and high surface area ceria, J. Catal. 193 (2000) 273–282.
[53] J.P. Holgado, R. Alvarez, G. Munuera, Study of CeO_2 XPS spectra by factor analysis: reduction of CeO_2, Appl. Surf. Sci. 161 (2000) 301–315.
[54] A.D. Logan, M. Shelef, Oxygen availability in mixed cerium/praseodymium oxides and the effect of noble metals, J. Mater. Res. 9-2 (1994) 468–475.
[55] R. Long, J. Luo, M. Chen, H. Wan, Oxidative coupling of methane over BaF_2-promoted rare earth oxides with variable valence, Appl. Catal. A Gen. 159 (1997) 171–185.
[56] M.F.L. Johnson, J. Mooi, Cerium dioxide crystallite sizes by temperature-programmed reduction, J. Catal. 103 (1987) 502–505.